

Supplemental Information

Architectural diversity in the solid-state behavior of crown ether and
[2.2.2]-cryptand complexes of $K^+TCNQ^{\bullet-}$ salts

Bingjia Yan^{a,b}, Peter N. Horton^a, Simon C. Weston^{a,c}, Christopher J. Wedge^d, Andrea E. Russell^a,
and Martin C. Grossel^{a*}

^a *School of Chemistry, University of Southampton, Highfield, Southampton, SO17 1 BJ, UK*

^b *Chemical Biology Department, Leibniz-Forschungsinstitut für Molekulare Pharmakologie (FMP), Robert-Rössle-Strasse 10, 13125 Berlin, Germany*

^c *ExxonMobil Technology & Engineering Company, Annandale, NJ 08801, USA*

^d *Department of Chemical Sciences, University of Huddersfield, Huddersfield, HD1 3DH, UK*

[†] *To whom correspondence should be addressed: Email: M.C.Grossel@soton.ac.uk; Fax: +44(0)*

23 8059 3781; Tel: +44(0) 23 8059 3153

Index

Table S1. Crystal structure data for ionophore alkali metal TCNQ complexes (1-5) in this study ...	3
Table S2. Key structural data for TCNQ dimers in the complexes (1-5) discussed here with comparative literature data (r.t. = room temperature, see Fig 3 for the definitions of long- and short-axis slippage).....	4
Fig S1. Side (A/C/E) and top (B/D/F) views of TCNQ units in (18-crown-6)K(TCNQ) _{2.5} (1).....	5
Fig S2. Side (A/C/E) and top (B/D/F) views of TCNQ units in (2.2.2-cryptand)K(TCNQ) _{2.5} (2).....	5
Fig S3. Side (A) and top (B) views of TCNQ units in (benzo-18-crown-6)K(TCNQ) ₂ (3).....	6
Fig S4. Side (A) and top (B) views of TCNQ units in (dibenzo-18-crown-6)K(TCNQ) ₂ (4).....	6
Fig S5. Side (A) and top (B) views of TCNQ units in (dicyclohexano-18-crown-6)K(TCNQ) ₃ (5).....	6
Fig S6. The EPR results of (18-crown-6)KTCNQ (6) re-measured for this study showing (A) angular dependence of the triplet exciton signals at 380K and (B) growth of the triplet exciton signals with increasing temperature for an arbitrary fixed orientation. Two spectral doublets arise from the crystallographically distinct TCNQ dimer columns. In both cases microwave power was 0.8 mW in a TM ₁₁₀ cavity with 0.50mT modulation amplitude used to aid observation of the small thermally populated exciton signals. The higher signal to noise in (B) is due to increased signal averaging necessary to discern the weak exciton signals at lower temperatures. Spectra were baseline corrected in MATLAB® using the EasySpin basecorr command to apply a second order polynomial correction. ⁴	7
Fig S7. Preliminary EPR of (2.2.2-cryptand)K(TCNQ) _{2.5} (2) at 295K showing (A) weak angular dependence of the anisotropic EPR signal and (B) power saturation with microwave attenuation values as shown. The signal varies in the linear regime (double intensity for 6 dB increase in power) for attenuations of 39 dB or more and while the complex lineshape changes at higher powers (lower attenuation) have not been fully interpreted they imply multiple overlapping signals, with decreasing intensity of the central component indicative of a long relaxation time. The angular dependence data in A is recorded for 39 dB attenuation (~25 μW microwave power). In both cases spectra were recorded in a TM ₁₁₀ cavity with 50 μT modulation amplitude and for clarity only the central portion of the 5.0mT sweep is shown.	7

TCNQ complex	1	2	3	4	5
CSD ref code	2119874	2119875	2119876	2119877	2119878
Empirical Formula	$C_{42}H_{34}KN_{10}O_6$	$C_{48}H_{46}N_{12}KO_6$	$C_{40}H_{32}N_8KO_6$	$C_{44}H_{32}N_8KO_6$	$C_{56}H_{48}N_{12}KO_6$
Formula (gmol ⁻¹)	813.89	926.07	759.84	807.87	1024.16
Crystal System, space group	Monoclinic, $P2_1/c$	Monoclinic, $P2_1/n$	Monoclinic, $P2_1/m$	Triclinic, $P-1$	Triclinic, $P-1$
a/Å	8.0740(2)	8.0104(2)	6.4442(1)	7.8459(3)	7.9514(2)
b/Å	31.7168(5)	36.7367(11)	35.1206(6)	14.5336(4)	9.9644(3)
c/Å	16.2190(3)	15.8116(4)	8.0868(2)	17.8334(4)	16.7703(4)
$\alpha/^\circ$	90	90	90	96.620(1)	87.136(2)
$\beta/^\circ$	100.863(2)	98.291(3)	99.840(2)	93.222(2)	79.011(2)
$\gamma/^\circ$	90	90	90	101.779(2)	80.148(3)
Vol/Å ³	4078.96(14)	4604.3(2)	1803.31(6)	1970.77(10)	1284.91(7)
Temperature (K)	100	100	100	120	100
D _x (gm ⁻³)	1.325	1.336	1.399	1.361	1.324
Abs coeff (mm ⁻¹)	0.191	0.179	0.209	0.196	0.168
Crystal	Shiny black	Shiny black	Dark blue	Black	Bright purple
Z	4	4	2	2	1
F000	1692.0	1940.0	790.0	838.0	535.0
h,k,lmax	10, 41, 21	10, 47, 20	8, 45, 10	10, 18, 23	10, 12, 21
R (reflections)	0.0353(7494)	0.0688(5909)	0.0332(3771)	0.0842(6598)	0.0350(5173)
wR ₂ (reflections)	0.0916(9358)	0.1632(10319)	0.0908(4212)	0.1698(8943)	0.0979(5852)

Table S1. Crystal structure data for ionophore alkali metal TCNQ complexes (1-5) in this study

Complex	TCNQ dimer	π - π separation/Å	Long-axis slippage/Å	Short-axis slippage/Å	Ref.
1. (at 100 K)	AC	3.17	2.12	0.32	This work
	AB	3.38	1.86	2.39	
2. (at 100 K)	AC	3.08	1.95	0.15	This work
	AB	3.24	1.96	0.38	
3. (at 100 K)	AA*	3.18	1.98	0.028	This work
4. (at 120 K)	AB	3.12	2.15	0.012	This work
5. (at 100 K)	AA'	3.05	2.17	0.015	This work
6. (at r.t.)	AB	3.23	0.08	0.33	1, 2
7. (ambient)	AB	3.15	0.03	1.00	3

Table S2. Key structural data for TCNQ dimers in the complexes (1-5) discussed here with comparative literature data (r.t. = room temperature, see Fig 3 for the definitions of long- and short-axis slippage).

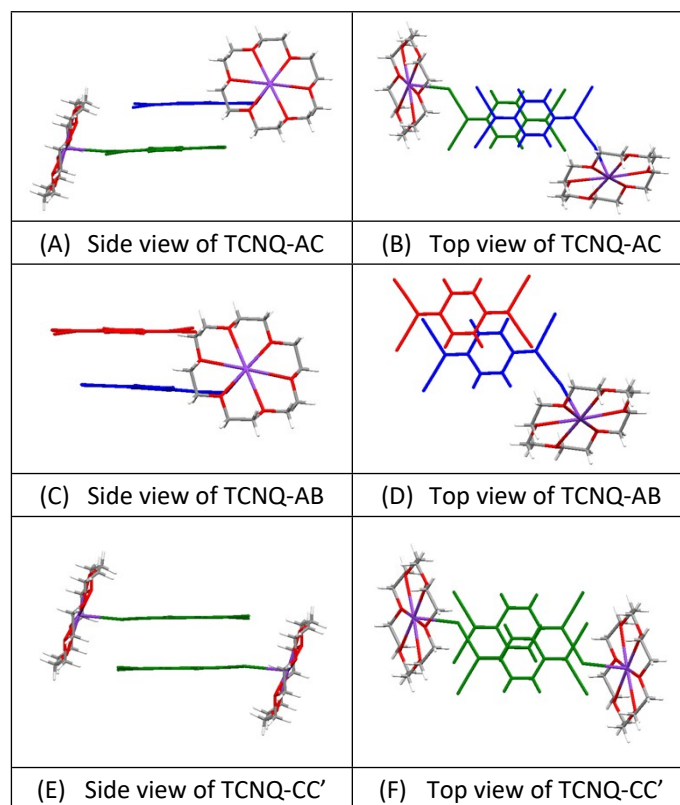


Fig S1. Side (A/C/E) and top (B/D/F) views of TCNQ units in (18-crown-6)K(TCNQ)_{2.5} (**1**).

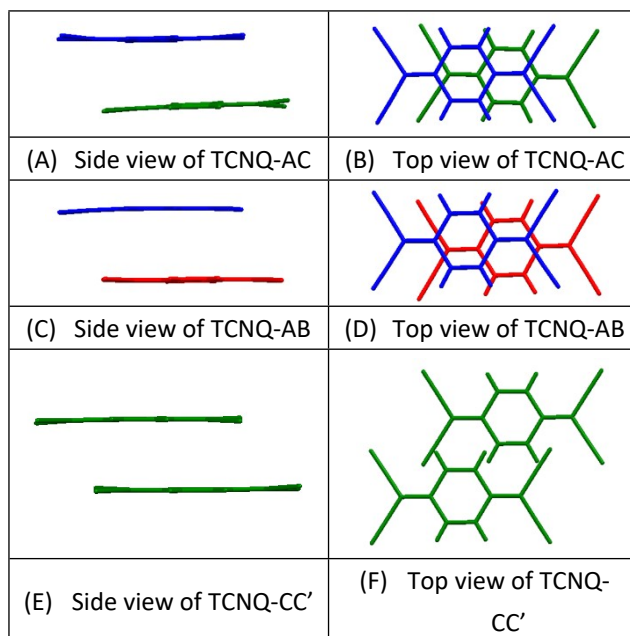


Fig S2. Side (A/C/E) and top (B/D/F) views of TCNQ units in (2.2.2-cryptand)K(TCNQ)_{2.5} (**2**).

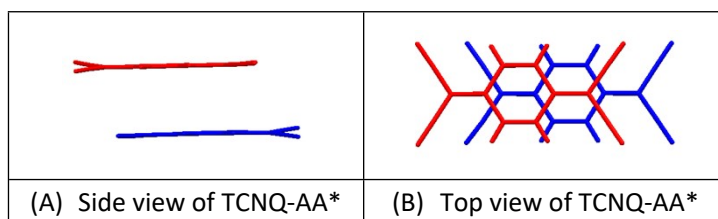


Fig S3. Side (A) and top (B) views of TCNQ units in (benzo-18-crown-6)K(TCNQ)₂ (**3**).

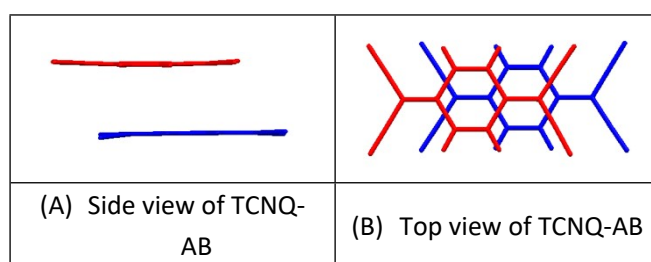


Fig S4. Side (A) and top (B) views of TCNQ units in (dibenzo-18-crown-6)K(TCNQ)₂ (**4**).

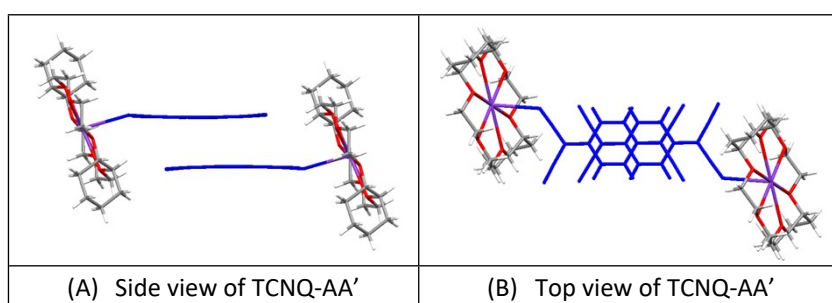


Fig S5. Side (A) and top (B) views of TCNQ units in (dicyclohexano-18-crown-6)K(TCNQ)₃ (**5**).

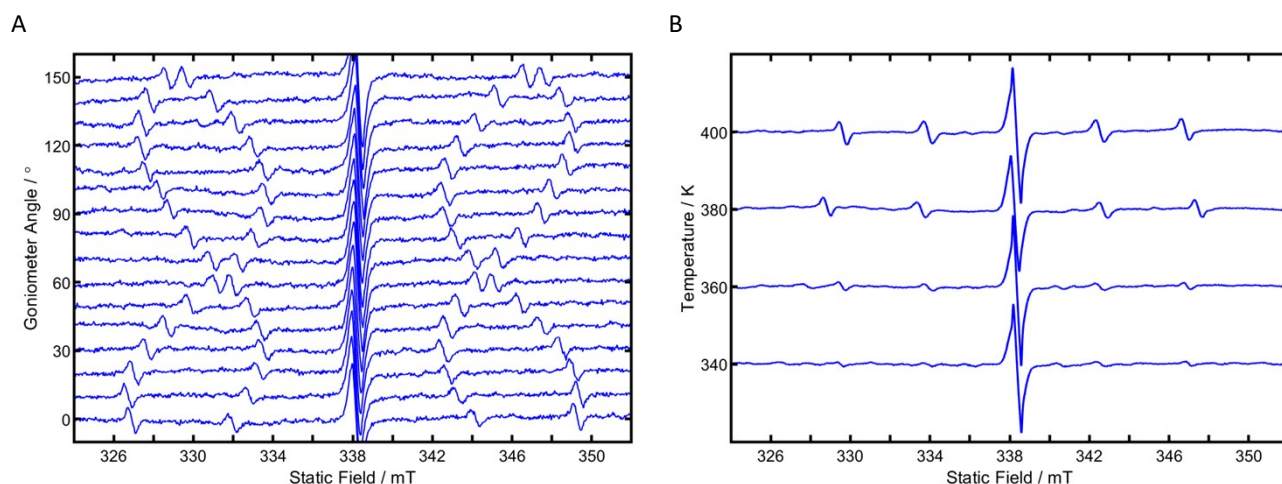


Fig S6. The EPR results of (18-crown-6)KTCNQ (**6**) re-measured for this study showing (A) angular dependence of the triplet exciton signals at 380K and (B) growth of the triplet exciton signals with increasing temperature for an arbitrary fixed orientation. Two spectral doublets arise from the crystallographically distinct TCNQ dimer columns. In both cases microwave power was 0.8mW in a TM_{110} cavity with 0.50mT modulation amplitude used to aid observation of the small thermally populated exciton signals. The higher signal to noise in (B) is due to increased signal averaging necessary to discern the weak exciton signals at lower temperatures. Spectra were baseline corrected in MATLAB® using the EasySpin `basecorr` command to apply a second order polynomial correction.⁴

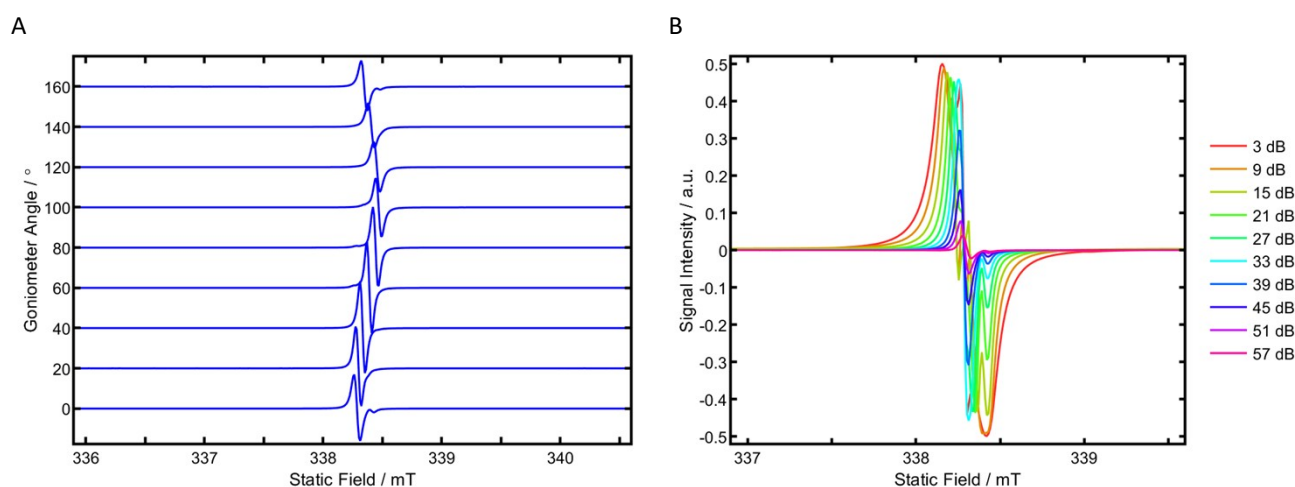


Fig S7. Preliminary EPR of (2.2.2-cryptand)K(TCNQ)_{2.5} (**2**) at 295 K showing (A) weak angular dependence of the anisotropic EPR signal and (B) power saturation with microwave attenuation values as shown. The signal varies in the linear regime (double intensity for 6 dB increase in power) for attenuations of 39 dB or more and while the complex lineshape changes at higher powers (lower attenuation) have not been fully interpreted they imply multiple overlapping signals, with decreasing intensity of the central component indicative of a long relaxation time. The angular dependence data in A is recorded for 39 dB attenuation ($\sim 25 \mu\text{W}$ microwave power). In both cases spectra were recorded in a TM_{110} cavity with $50 \mu\text{T}$ modulation amplitude and for clarity only the central portion of the 5.0 mT sweep is shown.

1. M. C. Grossel and S. C. Weston, *J. Phys. Org. Chem.*, 1992, **5**, 533-539.
2. R. C. Hynes, J. R. Morton, K. F. Preston, A. J. Williams, F. Evans, M. C. Grossel, L. H. Sutcliffe and S. C. Weston, *J. Chem. Soc., Faraday Trans.*, 1991, **87**, 2229-2233.
3. M. C. Grossel and S. C. Weston, *Chem. Mater.*, 1996, **8**, 977-980.
4. S. Stoll and A. Schweiger, *J. Magn. Reson.*, 2006, **178**, 42-55.